MultidirectionalSpin-Orbit Torque MagnetizationDynamics in beyond Room Temperature Van der Waals Magnet Devices

Citation for the original published paper (version of record):
Zhao, B., Bainsla, L., Ershadrad, S. et al (2026). MultidirectionalSpin-Orbit Torque
MagnetizationDynamics in beyond Room Temperature Van der
Waals Magnet Devices. Nano Letters, In Press. http://dx.doi.org/10.1021/acs.nanolett.6c02494

NANO LETTERS

pubs.acs.org/NanoLett
Letter

Multidirectional Spin−Orbit Torque Magnetization Dynamics in beyond Room Temperature Van der Waals Magnet Devices

Bing Zhao,*[,††] Lakhan Bainsla,[††] Soheil Ershadrad, Prabhav N. Sumant, Roselle Ngaloy, Johanna Rosen, Biplab Sanyal, Johan Åkerman, and Saroj P. Dash*

Cite This: https://doi.org/10.1021/acs.nanolett.6c02494

Read Online

ACCESS | Metrics & More | Article Recommendations | Supporting Information

ABSTRACT: van der Waals (vdW) magnets with room-temperature ferromagnetism offer exciting opportunities for energy-efficient spintronic devices, yet their magnetization dynamics remain largely unexplored despite their importance for high-speed memory technologies. Here, we investigate spin−orbit torque phenomena in the room-temperature vdW magnet $(Co_{0.15}Fe_{0.85})_5GeTe_2$ (CFGT)/Pt heterostructure using spin-torque ferromagnetic resonance and second-harmonic Hall measurements. Alongside a conventional in-plane spin Hall conductivity of 3.68×10^5 $(\hbar/2e)$ $(\Omega\ m)^{-1}$, we identify a sizable out-of-plane component of -0.33×10^5 $(\hbar/2e)$ $(\Omega\ m)^{-1}$ that generates unconventional damping-like torques. Density functional theory and Monte Carlo simulations suggest that this torque can originate from interface-induced spin reorientation arising from a modified magnetic anisotropy landscape and strongly enhanced Dzyaloshinskii−Moriya interaction at the CFGT/Pt interface. The combination of low effective magnetization (0.321 T), moderate Gilbert damping (0.027), and efficient multidirectional torques highlights vdW magnets as promising platforms for next-generation spintronic devices.

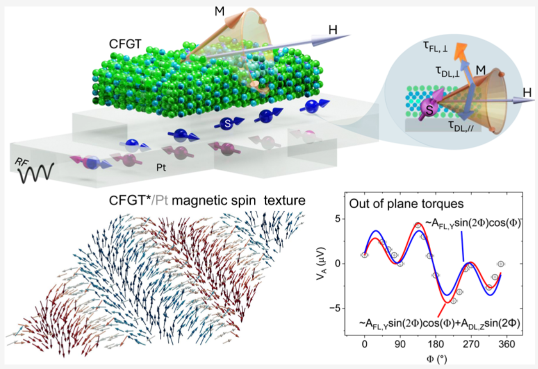

KEYWORDS: *spin−orbit torque (SOT), vdW magnets, 2D materials, room temperature, ST-FMR, second harmonic Hall, magnetization dynamics*

Continued technological advancements drive the need for smaller, faster, nonvolatile, and energy-efficient spintronic devices for information and communication technologies.[1,2] Spintronic memories based on spin-transfer torque (STT) phenomena have already been integrated into microcontrollers for autonomous systems, automobiles, space, gaming, artificial intelligence, and machine learning platforms.[3−5] In recent years, the chip industry has become interested in spin−orbit torque (SOT) nonvolatile memory for high-performance computing, due to its energy efficiency, faster speeds, and higher endurance and retention compared to its counterparts.[6−11] However, key challenges remain in achieving lower energy consumption, magnetic field-free operation, and tunability, necessary for widespread adoption in higher-level memory, memory-in-logic, and applications in artificial intelligence and neuromorphic computing.[4−6,12,13]

The emergence of two-dimensional (2D) vdW magnets has opened a new paradigm for spintronic device engineering because of ultralow dimensionality, tunable magnetic properties, and the ability to enable energy-efficient and field-free magnetization switching mechanisms.[14−18] Recent demonstrations of room-temperature vdW ferromagnets offer robust magnetization and a high degree of anisotropy control,[17,19] spanning both ferromagnetic and antiferromagnetic regimes,[17,19−23] as well as exotic spin textures[24,25] and coexisting magnetic orders.[26] These properties have enabled proof-of-concept magnetic tunnel junctions,[27−29] lateral spin-valves[22,23,25] and spin−orbit torque (SOT) memory devices.[26,30−35] However, systematic experimental studies of magnetization dynamics, specifically their spin−orbit torque efficiencies, magnetization damping, and charge-to-spin conversion, remain sparse but are essential for realizing fast and energy-efficient spintronic technologies.

Here, we report multidirectional SOT magnetization dynamics using the above room temperature vdW magnet $(Co_{0.15}Fe_{0.85})_5GeTe_2$ (CFGT) in heterostructure with Pt. Using both spin-torque ferromagnetic resonance (ST-FMR) in the frequency range of 2−14 GHz and second (2^{nd}) harmonic Hall measurement techniques, we observe a large in-plane spin Hall conductivity and a significant unconventional out-of-plane spin Hall conductivity. Further DFT calculations combined with Monte Carlo simulation show that proximity with Pt can introduce complex noncolinear spin textures in the

Received: May 22, 2026
Revised: June 27, 2026
Accepted: June 30, 2026

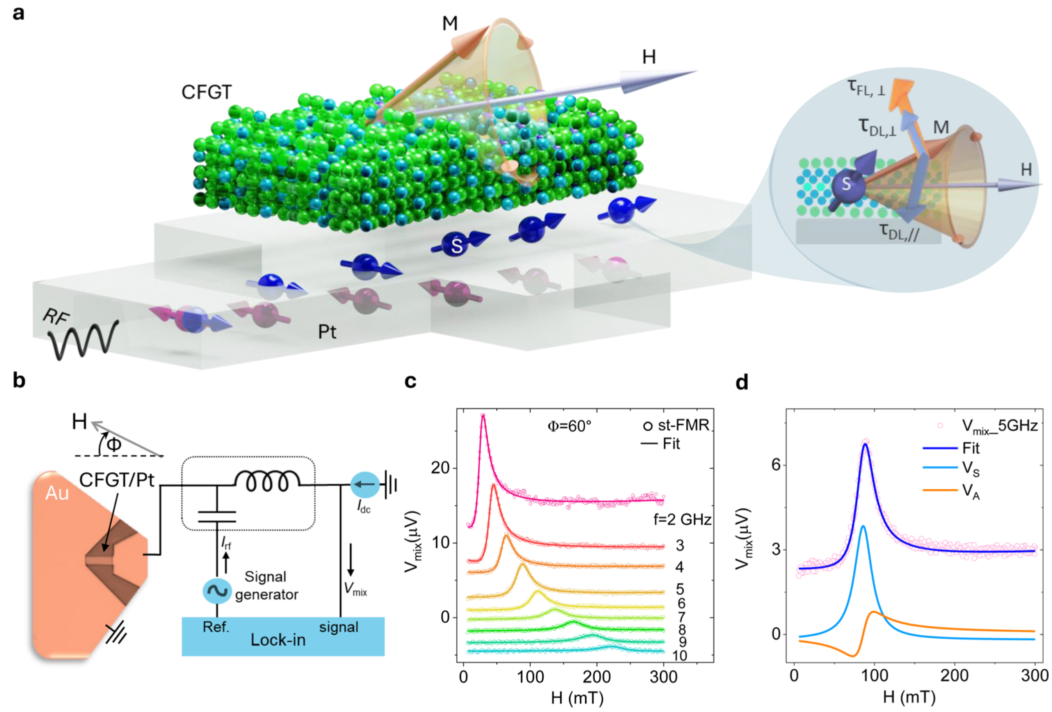

Figure 1. Magnetization dynamics measurements using CFGT/Pt heterostructure at room temperature. (a) Schematics of the CFGT/Pt heterostructure with magnetization M oscillation driven by SOTs and external B field. The inset shows the multidirectional spin current induced by conventional and unconventional SOT in the CFGT/Pt heterostructure. (b) Schematics of the spin-torque ferromagnetic resonance (ST-FMR) measurement setup with CFGT/Pt heterostructure device. (c) Representative ST-FMR data, showing V_{mix} as a function of the magnetic field at different radio frequencies in the range of f = 2−10 GHz at Φ = 60°. (d) ST-FMR signal at 5 GHz with the fitted symmetric (V_S) and antisymmetric (V_A) components. Measurements are performed on the CFGT(25 nm)/Pt(10 nm) ST-FMR device.

CFGT, which can be attributed to the strongly enhanced Dzyaloshinsky−Moriya interaction and weakened magnetic anisotropy energy with tilted magnetic easy axis. These results reveal crucial parameters governing efficient spin dynamics and unconventional SOT in vdW magnets for next-generation spintronic devices.

We were motivated to study magnetization dynamics in vdW magnet CFGT because of their above-room-temperature ferromagnetism with strong in-plane magnetic anisotropy.[22] Here, we employed the spin−orbit torque (SOT) induced ST-FMR and 2nd harmonic Hall measurements to investigate the magnetization dynamics of the vdW magnet CFGT/Pt heterostructure (Figure 1a). For the ST-FMR device fabrication, the CFGT crystals were first exfoliated onto a Si/SiO_2 substrate inside a glovebox, followed by Pt deposition to create the CFGT/Pt heterostructure (see the Methods section). Subsequently, the CFGT/Pt heterostructure was patterned into rectangular microbar devices with an integrated microwave guide with Ti/Au contacts for the ST-FMR measurements (Figure 1b). The acquired measurements unveiled information about effective magnetization $\mu_0 M_{eff}$, effective Gilbert damping constant α, magnetic anisotropy H_k, and SOT efficiency at room temperature.

In ST-FMR measurements, an in-plane radio-frequency (RF) current I_{RF} is applied along the CFGT/Pt stripe, while an in-plane magnetic field H is applied at an angle Φ with respect to the I_{RF}. The spin−orbit coupling in Pt generates a spin current perpendicular to the direction of I_{RF}, which is injected into the adjacent CFGT layer and exerts a torque on the magnetization of CFGT, causing it to precess. The I_{RF} causes the anisotropic magnetoresistance (AMR) to oscillate and produces a DC mixing voltage V_{mix}, which is then measured using a lock-in amplifier. The representative ST-FMR signals V_{mix} for the CFGT/Pt device at room temperature are shown in Figure 1c. The obtained V_{mix} is fitted by eq 1,[36−38]

$$V_{mix} = V_S F_S(H) + V_A F_A(H) \quad (1)$$

where $F_S(H) = \frac{\Delta H^2}{\Delta H^2 + (H - H_R)^2}$ and $F_A(H) = F_S(H)\left[\frac{(H - H_R)}{\Delta H}\right]$ are symmetric and antisymmetric Lorentzian functions, respectively. H, ΔH, and H_R are the applied external magnetic field, ferromagnetic resonance line width, and ferromagnetic resonance field, respectively. V_S and V_A are the amplitudes of symmetric and antisymmetric signals and are proportional to the current-induced in-plane torque and out-of-plane torque, respectively.[39] The obtained V_{mix} at 5 GHz is shown in Figure 1d, where symmetric and antisymmetric components are extracted and shown for reference. The extracted values of ΔH and H_R are used to obtain the effective magnetization $\mu_0 M_{eff}$, by fitting the frequency f versus H_R data to the Kittel equation[38,40,41] $f = \left(\frac{\gamma}{2\pi}\right)\mu_0\sqrt{(H_R - H_k)(H_R - H_k + M_{eff})}$ as given in Figure 2a. The Gilbert damping constant α is evaluated by fitting the ΔH versus f using $\Delta H = \Delta H_0 + \frac{2\pi\alpha f}{\gamma}$, as shown in Figure 2b. The $\mu_0 M_{eff}$ = 0.321 ± 0.014 T and α = 0.027 ± 0.001 are obtained for the CFGT/Pt device, as given in parts a and b of Figure 2, respectively (additional results at Φ = 240° are presented in Supplementary Figure S1).

To estimate the effective damping-like SOT efficiency, the DC bias-dependent ST-FMR measurements are done on the ST-FMR device as well, and the representative data at different values of DC current (I_{dc}) are shown in Figure 2c,d. The resonance line width, ΔH at different I_{dc} is extracted, and

https://doi.org/10.1021/acs.nanolett.6c02494
Nano Lett. XXXX, XXX, XXX−XXX

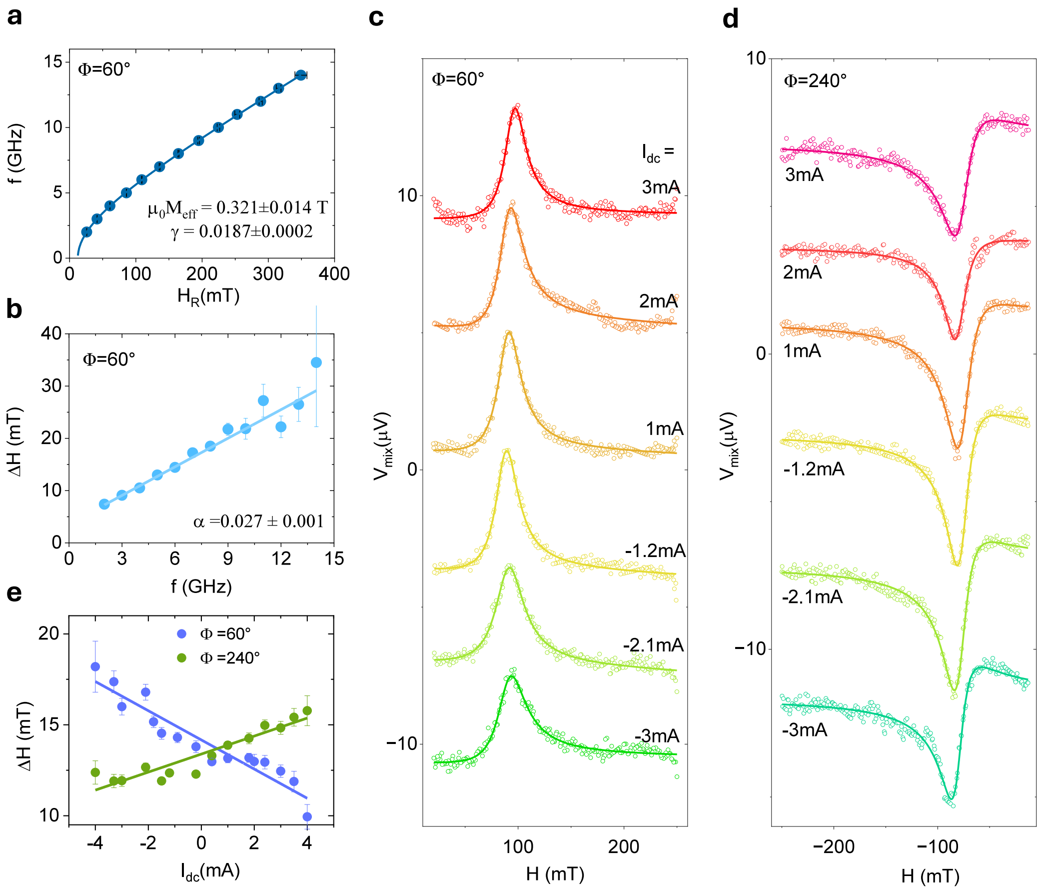

Figure 2. Evaluation of magnetization dynamic parameters and effective spin−orbit torque efficiency from DC bias-dependent ST-FMR measurements. (a) Fitting of resonant frequency f versus the extracted resonant field H_R. (b) Fitting of resonant extracted line width ΔH versus resonant frequency f (GHz). The error bars are calculated from the standard deviation of the signal background. (c and d) DC current tuned ST-FMR plots for positive/negative fields at a frequency of 5 GHz using different values of I_{dc}. Hollow dots denote experimental data while solid lines correspond to fitting performed using eq 1. (e) Line width versus DC current plot at 5 GHz for positive (blue line) and negative (dark green line) fields. The fitted slope of these lines is used to calculate the SOT efficiency of damping-like torque using eq 2. All the solid curves are the fitting results.

shown in Figure 2e. The strength of damping-like SOT efficiency is estimated using the slope of linearly fitted ΔH versus I_{dc} data,[36−38]

$$\xi_{DL}^{eff} = \frac{2e}{\hbar}\frac{(H_R + 0.5M_{eff})\mu_0 M_S t_{CFGT}}{\sin\phi}\frac{\gamma}{2\pi f}\frac{\delta\Delta H}{\delta(I_{dc,Pt})}A_C \quad (2)$$

where Φ is the azimuthal angle between I_{dc} and H. M_{eff}, $\mu_0 M_S$, t_{CFGT}, and $\frac{\gamma}{2\pi}$ are the effective magnetization, saturation magnetization, thickness, and effective gyromagnetic ratio of the CFGT layer, respectively. e and $\hbar$ are the elementary charge and the reduced Planck's constant. $I_{dc,Pt}$ is the current in the Pt layer, and A_C is the cross-sectional area of the ST-FMR microbars. The effective spin Hall conductivity ($\sigma_{SHC} = \sigma_c \xi_{DL}^{eff}$) values are evaluated to be 1.13 × 10^6 ($\hbar$/2e) (Ω m)$^{-1}$ for CFGT/Pt heterostructure. Noticeably, the effective SOT efficiency value obtained from DC bias-dependent measurements might have unwanted contributions due to thermal effects, which could result in deviations in SOT efficiency compared to its intrinsic values.[42]

To gain more insight into different SOT components, we also performed the in-plane angle dependence of the ST-FMR measurements, as shown in Figure 3a,b. The symmetric (V_S) and antisymmetric (V_A) components are extracted by fitting the ST-FMR signals at different in-plane angles Φ with eq 1, as illustrated in Figure 3c,d. Traditionally, the relation of the symmetric and antisymmetric components as a function of the in-plane angle Φ can be expressed as follows:[39,43]

$$V_S = S_{DL,Y}\sin(2\Phi)\cos(\Phi) \quad (3)$$

$$V_A = A_{FL,Y}\sin(2\Phi)\cos(\Phi) \quad (4)$$

$S_{DL,Y}$ and $A_{FL,Y}$ are the coefficients for the damping and field-like torques with spin polarizations along the y direction. However, we found that the antisymmetric component is not fitted properly with eq 4 (blue curve in Figure 3d). Then another term $A_{DL,Z}\sin(2\Phi)$ was added in eq 4, and we have

$$V_{A1} = A_{FL,Y}\sin(2\Phi)\cos(\Phi) + A_{DL,Z}\sin(2\Phi) \quad (5)$$

$A_{DL,Z}$ is the coefficient for the damping-like torque with spin polarizations along the z direction. The new formula (eq 5) shows a better fitting result (red curve in Figure 3d), which suggests the presence of an additional out-of-plane SOT component (see a more detailed analysis in Supplementary Note 1, Supplementary Figure S2, and Table S1). The in-plane ($\xi_{DL,j}^{Y}$) and out-of-plane ($\xi_{DL,j}^{Z}$) damping-like torque efficiencies per unit current density could be extracted using

https://doi.org/10.1021/acs.nanolett.6c02494
Nano Lett. XXXX, XXX, XXX−XXX

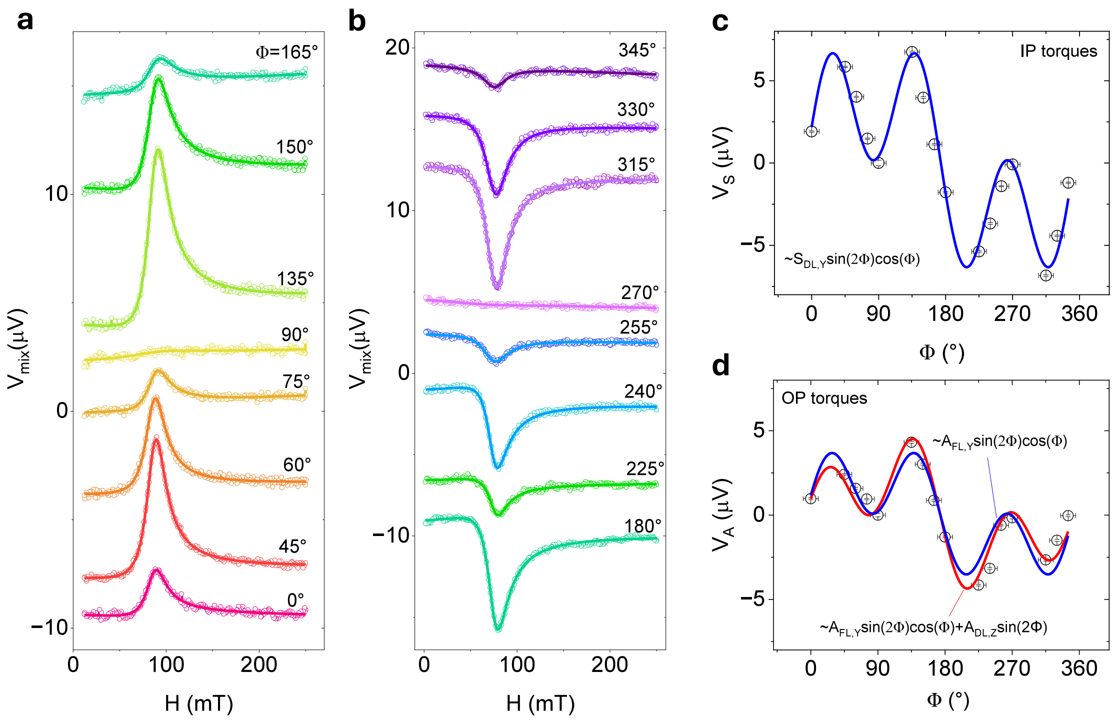

Figure 3. Unconventional spin–orbit torque in CFGT/Pt heterostructures from angular ST-FMR measurements. (a and b) Angular dependence of the ST-FMR signals at a frequency of 5 GHz. The open circles denote the output V_{mix} signal, and the solid lines represent the fitting by eq 1. (c and d) Angular dependence of the extracted symmetric component V_S and antisymmetric component V_A, respectively. Solid curves denote the fitting to the data using equations indicated in the figures.

$$\xi_{DL,j}^{Y} = \frac{S_{DL,Y}}{A_{FL,Y}}\frac{e\mu_0 M_S t_{Pt} t_{FM}}{\hbar}\sqrt{1+\frac{M_{eff}}{H_R}} \tag{6}$$

$$\xi_{DL,j}^{Z} = \frac{A_{DL,Z}}{A_{FL,Y}}\frac{e\mu_0 M_S t_{Pt} t_{FM}}{\hbar} \tag{7}$$

The in-plane and out-of-plane damping-like torque efficiencies of $\theta_{SH,Y} = 0.147 \pm 0.015$ and $\theta_{SH,Z} = -0.013 \pm 0.005$ are obtained for spin polarization S_y and S_z, respectively. Correspondingly, the effective spin Hall conductivity components are evaluated to be $\sigma_{SH,Y} = 3.68 \times 10^5$ $(\hbar/2e)$ $(\Omega\ m)^{-1}$ and $\sigma_{SH,Z} = -0.33 \times 10^5$ $(\hbar/2e)$ $(\Omega\ m)^{-1}$, respectively, which are comparable with $TaIrTe_4$[44,45] and $PtTe_2/WTe_2$[46] and larger than WTe_2.[39] Interestingly, such an unconventional out-of-plane damping-like torque component is observed in the CFGT/Pt heterostructure using ST-FMR measurements.

To further verify this unconventional torque, we performed second harmonic Hall measurements in microfabricated Hall bar devices (see Figure 4a and the Methods section). Specifically, the in-plane angle dependence harmonic Hall measurement is used to extract the effective spin–orbit field $H_{DL(FL)}$ along *x*-, *y*-, and *z*-axis directions and thermal contributions V_{th} with the 2nd harmonic Hall voltage

$$V_{xy}^{2\omega} = D_{DL,Y}\cos(\Phi) + D_{DL,Z}\cos(2\Phi) + F_{FL,Y}\cos(2\Phi)\cos(\Phi) + F_{FL,Z} \tag{8}$$

where

$$D_{DL,Y} = -\frac{H_{DL,Y}V_{AHE}}{2(H+Hk)} + V_{th} \tag{9}$$

$$D_{DL,Z} = -\frac{H_{DL,Z}V_{PHE}}{H} \tag{10}$$

$$F_{FL,Y} = -\frac{H_{FL,Y}V_{PHE}}{H} \tag{11}$$

Φ is the angle between the applied current I_{ac} and the magnetic field *H*. V_{AHE} and V_{PHE} are the AHE voltage and planar Hall (PHE) voltage, respectively. V_{th} is the thermal-related contribution, like anomalous Nernst and spin Seebeck effects, and H_k is the magnetic anisotropy field. By measuring the in-plane angle dependence of the first harmonic signal $V_{xy}^{1\omega}$ at a fixed large in-plane field, we can extract the V_{PHE} with $R_{xy}^{1\omega} = R_{PHE}\sin(2\Phi) + R_{AHE}\cos(\Phi) + c$ (as shown in Figure 4b). The 2nd harmonic signal $V_{xy}^{2\omega}$ in Figure 4c can be fitted with eq 8. The extracted components $F_{FL,Y}$ and $D_{DL,Y(Z)}$ as a function of the external field are plotted in Figure 4d,e. To further evaluate the effective fields induced by the SOT, eqs 9–11 are adopted, respectively. The bias dependence of the effective fields and thermal contribution are presented in (Figure 4f), which exhibit strong linear and parabolic relations with the bias current, respectively.

Because the damping-like torque is attributed to the longitudinal spin–orbit effective field H_{DL}, the spin–orbit efficiency can be calculated.[47,48]

$$\xi_{DL,Y(Z)} = T_{ini}\theta_{SH} = \frac{2e}{\hbar}\mu_0 M_S t_{CFGT}^{eff} H_{DL,Y(Z)}/J_{ac} \tag{12}$$

where J_{ac} is the current density of Pt, e is the electron charge, ℏ is the reduced Planck constant, and $\mu_0 M_S$ and t_{CFGT}^{eff} are the saturation magnetization and the effective thickness of CFGT, respectively. By assuming the fully transparent interface, i.e., $T_{ini} = 1$, and effective saturation magnetization $\mu_0 M_S = \mu_0 M_{eff}$,

https://doi.org/10.1021/acs.nanolett.6c02494
Nano Lett. XXXX, XXX, XXX−XXX

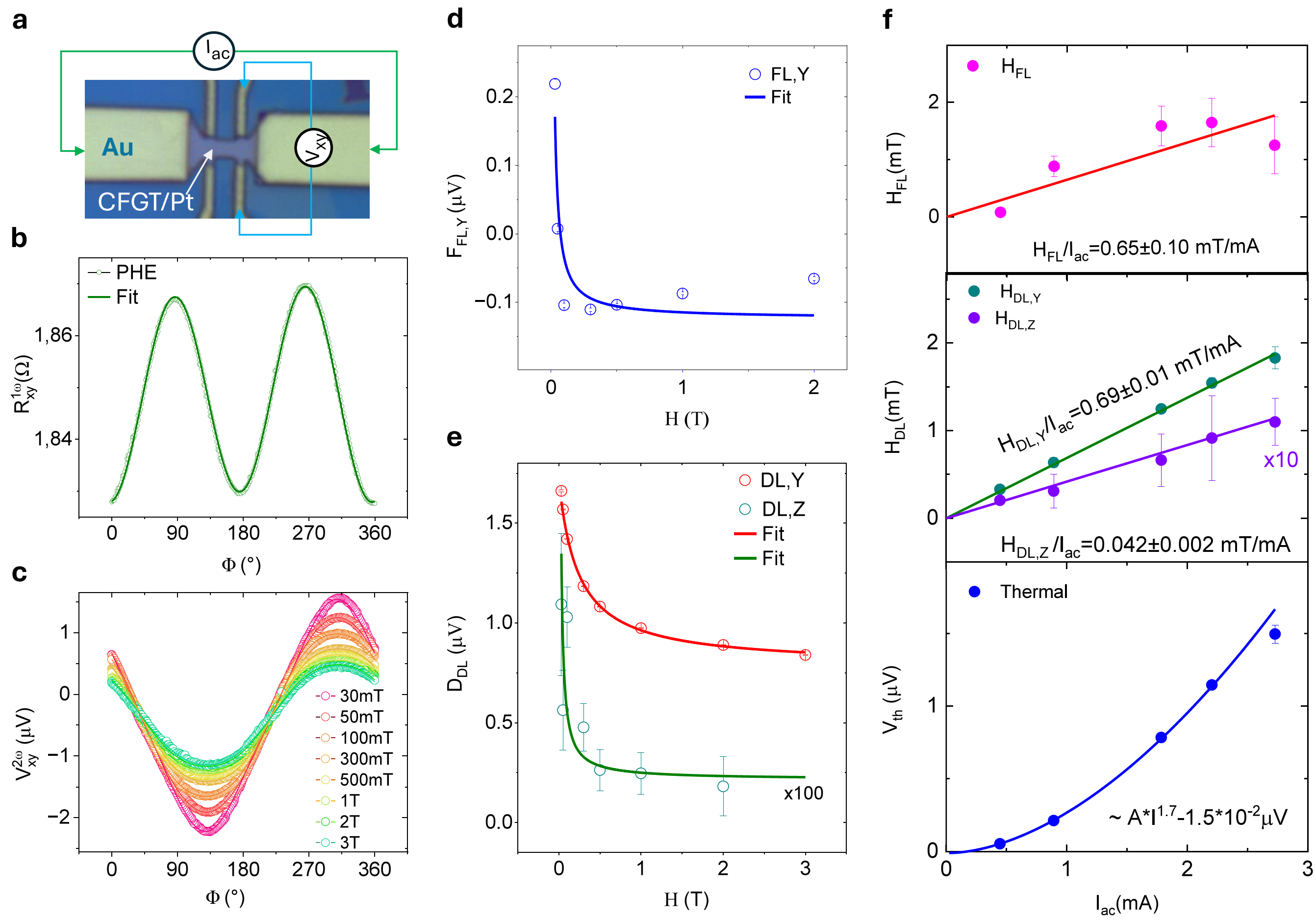

Figure 4. Harmonic measurements of the CFGT/Pt heterostructure at room temperature. (a) Schematics of the harmonic measurement setup with CFGT(15 nm)/Pt(10 nm) heterostructure Hall bar device. (b) First harmonic signal as a function of the in-plane angle with H_{ip} = 1 T and fitting result (solid curve). (c) In-plane angle dependence of the 2nd harmonic signals with different fields and corresponding fitting (solid) curves at I_{ac} = 1.78 mA. (d and e) Extracted effective H_{FL} and D_{DL} components as a function of the external field with fitting results. (f) Extracted effective field H_{FL}, H_{DL}, and thermal contribution as a function of the bias currents. The solid curves are the linear and nonlinear fitting results.

we obtain spin Hall angle $\theta_{SH,Y}$ = 0.157 ± 0.002 and $\sigma_{SH,Y}$ = (3.93 ± 0.05) × 10^5 (ℏ/2e) $(\Omega\ m)^{-1}$ and $\theta_{SH,Z}$ = 0.010 ± 0.001 and $\sigma_{SH,Z}$=(0.23 ± 0.03) × 10^5 (ℏ/2e) $(\Omega\ m)^{-1}$, which are comparable to the results obtained from ST-FMR experiments.

Our study of mechanisms governing magnetization dynamics and SOT in vdW magnet CFGT with in-plane magnetic anisotropy at room temperature uncovers their unique and unconventional spin−orbit torque behavior. Both ST-FMR and second harmonic Hall measurements show that the SOT efficiency of CFGT/Pt along S_y polarization is comparable to that of the other vdW magnets in a heterostructure with Pt.[26,31−34,49] However, in addition, a large unconventional SOT component S_z is also observed. Our control experiments of a single CFGT nanolayer with second harmonic Hall measurements prove that the self-torque from the single CFGT nanolayers can be ruled out (see detailed results in Supplementary Note 2 and Supplementary Figure S3). Furthermore, Pt is a well-studied SOT material with a dominant S_y component, so any bulk material-related unconventional SOT effects can be ruled out. Furthermore, our previous study on CFGT/graphene[22] suggests that the in-plane magnetic anisotropy of CFGT is independent of thickness variation. Therefore, the unconventional spin component should not originate from bulk CFGT, but rather from an interface-driven phenomenon. To confirm this, our DFT calculations combined with Monte Carlo simulation show that proximity with Pt introduces complex noncolinear spin textures in the CFGT (Figure 5a,b), which can be attributed to the strongly enhanced Dzyaloshinsky−Moriya interaction (Supplementary Figures S5 and S6), and weakened magnetic anisotropy energy with tilted magnetic easy axis (∼16°; Figure 5c and Supplementary Figure S4). This is in contrast to the pristine CFGT, which exhibits in-plane magnetic anisotropy, consistent with our previous experimental results (see a more detailed discussion in Supplementary Note 3). These observations suggest that the reported unconventional torque is not specific to a particular thickness or a single surface but is instead a robust feature of the CFGT/Pt interface.

Although such interface-related spin reorientation phenomena in conventional ferromagnetic materials heterostructures have been reported before, the origin remains elusive.[50−52] Here, we show that the modified magnetic anisotropy and interfacial DMI at the CFGT/Pt interface can induce the spin reorientation toward an unconventional spin polarization, in addition to the traditional spin Hall effect-induced counterpart (Figure 5c, bottom panel). This largely expands the library for multiple spin polarization mechanisms (Figure 5d), including (1) lower crystal symmetry related SHE (such as WTe_2,[39,53,54]

https://doi.org/10.1021/acs.nanolett.6c02494
Nano Lett. XXXX, XXX, XXX−XXX

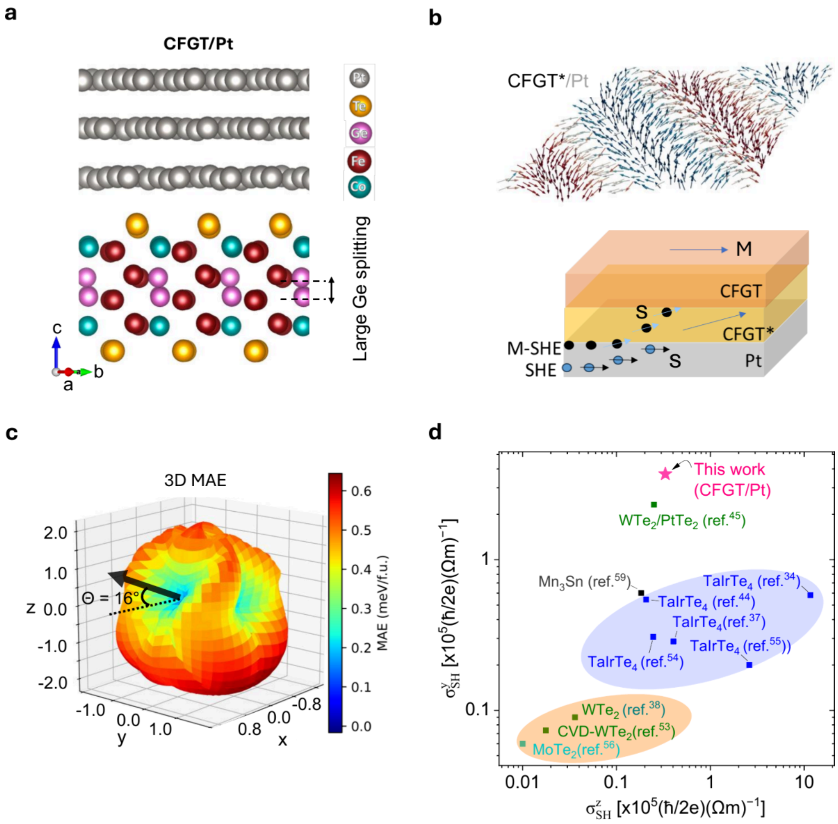

Figure 5. Theoretical calculations: DFT and Monte Carlo simulation results for CFGT/Pt heterostructure. (a) Schematic illustration of the relaxed geometry of CFGT/Pt atomic crystal structures. (b) Top panel: Monte Carlo simulation of the magnetic spin textures of CFGT/Pt. Bottom panel: Schematic illustration of the spin Hall effect (SHE) induced in-plane spin polarization and titled magnetic dependent spin Hall effect induced the unconventional spin component in modified CFGT interfaced with Pt. (c) 3D magnetic anisotropy energy (MAE) of CFGT/Pt. (d) State-of-the-art spin Hall conductivity in representative SOT devices with multiple spin polarizations.

$TaIrTe_4$,[35,38,39,45,55,56] and $MoTe_2$[57]), (2) spin swapping effect,[46] which converts the in-plane spin polarization to the out-of-plane one due to crystal asymmetry, (3) broken time-reversal symmetry (ferromagnetic moments) related effects, such as the anomalous spin Hall effect.[58−60]

We further compare the magnetization dynamics parameters of CFGT with other vdW magnets (like Fe_xGeTe_2)[61,62] and conventional magnetic thin films ($Ni_{80}Fe_{20}$, CoFeB).[63−66] The CFGT damping constant is lower than that of other vdW magnets, while relatively higher than that of conventional magnetic thin films. However, vdW magnets, due to their layered nature, could host a larger magnetic anisotropy H_k without dealing with the traditional thin films' complicated interface engineering.[65,66] In particular, CFGT exhibits strong in-plane anisotropy and a relatively lower damping constant α at room temperature, which has high potential for magnetization dynamic applications. It reveals a previously unexplored symmetry-breaking mechanism at the CFGT/Pt interface and expands the understanding of how different torque components can emerge in vdW heterostructures. These findings are expected to be highly relevant for future studies aiming to engineer magnetic anisotropy, enable deterministic switching in related systems, or utilize such unconventional torques in other magnetic configurations. Moreover, although out-of-plane magnets are preferred for the high-density SOT magnetic random-access memory (MRAM) technology to replace the high capacity of dynamic random-access memory (RAM) cells, however, in-plane magnets with larger endurance and faster magnetization dynamics should be sufficient to replace static RAM and cache memory applications, where speed is more important than density.

In conclusion, we observed multidirectional magnetization dynamics with a significant SOT efficiency using vdW magnet CFGT in a heterostructure with Pt at room temperature. Both ST-FMR and second harmonic Hall experiments reveal large charge-to-spin conversion and damping-like SOT efficiencies, with observation of an unconventional out-of-plane spin Hall conductivity, an effect distinct from conventional ferromagnet/Pt heterostructures. This unconventional torque component, which manifests as an additional damping-like torque with out-of-plane spin polarization, is expected to originate from interface-driven spin reorientation effects, due to strong interfacial DMI and modified MAE landscape. The extracted magnetization dynamics parameters, effective magnetization of 0.321 T and Gilbert damping constant of 0.027, position CFGT as a competitive platform for spintronic devices. These findings on spin dynamics in vdW magnetic heterostructures indicate that interface engineering may enable pathways to nonvolatile spintronic devices with enhanced functionality.[67]

METHODS

Device Fabrication

The van der Waals crystals of CFGT were grown by HqGraphene. The CFGT samples were prepared by mechanically exfoliating onto a SiO_2/Si wafer using the Scotch tape method inside a glovebox. Pt was deposited by electron beam evaporation after 15 s of Ar plasma cleaning to fabricate CFGT/Pt heterostructures. The CFGT/Pt heterostructures were then patterned into the rectangular microstrips for ST-FMR measurements and Hall bars for harmonic measurements using the Ar ion milling with e-beam resist as the etching mask.

Anisotropic Magnetoresistance Measurements

In-plane angular dependence, anisotropic magnetoresistance (AMR) measurements are performed on microbars using a rotatable projected vector field magnet with a fixed applied magnetic field of 1 T and applied DC current of 0.5 mA. The resistance of the devices was measured while rotating the magnetic field in the plane.

Spin Torque Ferromagnetic Resonance (ST-FMR) Measurements

ST-FMR measurements are performed at room temperature on the microbar devices to estimate the spin−orbit torque (SOT) efficiency and other magnetodynamical parameters. The measurements for effective SOT analysis are performed with a fixed in-plane angle ϕ = 60°, the radio-frequency (RF) current modulated at 98.76 Hz is applied to the device through a high-frequency bias-T at a fixed frequency (ranging from 3 to 14 GHz) with an input RF power P = 4 dBm. The in-plane angle ϕ dependence ST-FMR measurements are performed using a rotatable projected field magnet with ϕ = 0−360° (step of 15°) at a fixed frequency.

2nd Harmonic Hall measurements

The 2nd harmonic measurements in the high magnetic field range were carried out in the Quantum Design DynaCool PPMS system with an external electronic connection to Lockin SR830 to measure the first and second harmonic voltages with fixed frequency ω = 213.34 Hz.

■ ASSOCIATED CONTENT

Data Availability Statement

The data supporting the findings of this study are available from the corresponding authors upon reasonable request.

Supporting Information

The Supporting Information is available free of charge at https://pubs.acs.org/doi/10.1021/acs.nanolett.6c02494.

Analysis of ST-FMR results (Supplementary Note 1), control experiments for self-torque in CFGT (Supplementary Note 2), magnetic dynamic parameters of this work at room temperature (Supplementary Table S1), and DFT supplemental results (Supplementary Note 3) (PDF)

■ AUTHOR INFORMATION

Corresponding Authors

Saroj P. Dash − *Department of Microtechnology and Nanoscience, Chalmers University of Technology, SE-41296 Göteborg, Sweden; Wallenberg Initiative Materials Science for Sustainability and Graphene Center, Chalmers University of Technology, SE-41296 Göteborg, Sweden;* orcid.org/0000-0001-7931-4843; Email: saroj.dash@chalmers.se

Bing Zhao − *Department of Microtechnology and Nanoscience, Chalmers University of Technology, SE-41296 Göteborg, Sweden;* orcid.org/0000-0002-5560-6750; Email: zbing@chalmers.se

Authors

Lakhan Bainsla − *Department of Microtechnology and Nanoscience, Chalmers University of Technology, SE-41296 Göteborg, Sweden; Department of Physics, Indian Institute of Technology Ropar, Roopnagar 140001, India;* orcid.org/0000-0001-9626-4278

Soheil Ershadrad − *Department of Physics, Thin Film Physics, Chemistry and Biology (IFM), Linköping University, Linköping SE-58183, Sweden; Wallenberg Initiative Materials Science for Sustainability (WISE), Department of Physics, Chemistry and Biology (IFM), Linköping University, Linköping 58183, Sweden*

Prabhav N. Sumant − *Department of Microtechnology and Nanoscience, Chalmers University of Technology, SE-41296 Göteborg, Sweden*

Roselle Ngaloy − *Department of Microtechnology and Nanoscience, Chalmers University of Technology, SE-41296 Göteborg, Sweden*

Johanna Rosen − *Department of Physics, Thin Film Physics, Chemistry and Biology (IFM), Linköping University, Linköping SE-58183, Sweden; Wallenberg Initiative Materials Science for Sustainability (WISE), Department of Physics, Chemistry and Biology (IFM), Linköping University, Linköping 58183, Sweden;* orcid.org/0000-0002-5173-6726

Biplab Sanyal − *Department of Physics and Astronomy, Uppsala University, Uppsala SE-75120, Sweden;* orcid.org/0000-0002-3687-4223

Johan Åkerman − *Department of Physics, University of Gothenburg, SE-41296 Göteborg, Sweden; Center for Science and Innovation in Spintronics and Research Institute of Electrical Communication, Tohoku University, Aoba-ku, Sendai 980-8577, Japan;* orcid.org/0000-0002-3513-6608

Complete contact information is available at: https://pubs.acs.org/10.1021/acs.nanolett.6c02494

Author Contributions

[††]B.Z. and L.B. contributed equally to this work. B.Z. and L.B. fabricated and measured the devices with the help of P.N.S. and R.N.. S.E., J.R., and B.S. performed theoretical calculations and analysis. B.Z., L.B., J.Å., and S.P.D. analyzed and interpreted the experimental data and wrote the manuscript with comments from all of the authors. S.P.D. coordinated and supervised the project.

Notes

The authors declare no competing financial interest.

■ ACKNOWLEDGMENTS

The authors acknowledge funding from European Innovation Council (EIC) Project 2DSPIN-TECH (No. 101135853), European Commission Graphene Flagship project, 2D TECH VINNOVA competence center (No. 2019-00068), KAW, Wallenberg initiative on Materials Science for a Sustainable World (WISE), FLAG-ERA Projects 2DSOTECH (VR No. 2021-05925) and MagicTune (No. 2023-06210), Swedish Research Council (VR) grants (Nos. 2025-03702 and 2021-04821), Graphene Center, AoA Nano, Chalmers-Max IV collaboration grant, AoA Energy and AoA Materials program at Chalmers University of Technology. L.B. acknowledges funding from Ministry of Electronics and Information Technology (Meity) (Grant no. 3149159). The fabrication of devices was performed at Nanofabrication laboratory MyFab at Chalmers University of Technology. J.R. and S.E. acknowledge WISE through KAW. B.S. acknowledges financial support from the Swedish Research Council (Grant 2022-04309) and STINT Mobility Grant for Internationalization (Grant MG2022-9386). B.S. also acknowledges computational resources provided by the National Academic Infrastructure for Supercomputing in Sweden (NAISS) at UPPMAX (NAISS

2025/2-468) and at NSC and PDC (NAISS 2025/3-68), partially funded by the Swedish Research Council through Grant Agreement 2022-06725.

REFERENCES

(1) Lin, X.; Yang, W.; Wang, K. L.; Zhao, W. Two-Dimensional Spintronics for Low-Power Electronics. *Nat. Electron.* **2019**, *2* (7), 274−283.

(2) Yang, H.; Valenzuela, S. O.; Chshiev, M.; Couet, S.; Dieny, B.; Dlubak, B.; Fert, A.; Garello, K.; Jamet, M.; Jeong, D.-E.; Lee, K.; Lee, T.; Martin, M.-B.; Kar, G. S.; Sénéor, P.; Shin, H.-J.; Roche, S. Two-Dimensional Materials Prospects for Non-Volatile Spintronic Memories. *Nature* **2022**, *606* (7915), 663−673.

(3) Guo, Z.; Yin, J.; Bai, Y.; Zhu, D.; Shi, K.; Wang, G.; Cao, K.; Zhao, W. Spintronics for Energy- Efficient Computing: An Overview and Outlook. *Proc. IEEE* **2021**, *109* (8), 1398−1417.

(4) Yang, J.-Q.; Wang, R.; Ren, Y.; Mao, J.-Y.; Wang, Z.-P.; Zhou, Y.; Han, S.-T. Neuromorphic Engineering: From Biological to Spike-Based Hardware Nervous Systems. *Adv. Mater.* **2020**, *32* (52), 2003610.

(5) Capra, M.; Peloso, R.; Masera, G.; Ruo Roch, M.; Martina, M. Edge Computing: A Survey On the Hardware Requirements in the Internet of Things World. *Future Internet* **2019**, *11* (4), 100.

(6) Shao, Q.; Li, P.; Liu, L.; Yang, H.; Fukami, S.; Razavi, A.; Wu, H.; Wang, K.; Freimuth, F.; Mokrousov, Y.; Stiles, M. D.; Emori, S.; Hoffmann, A.; Akerman, J.; Roy, K.; Wang, J.-P.; Yang, S.-H.; Garello, K.; Zhang, W. Roadmap of Spin-Orbit Torques. *IEEE Trans. Magn.* **2021**, *57* (7), 1−39.

(7) Oboril, F.; Bishnoi, R.; Ebrahimi, M.; Tahoori, M. B. Evaluation of Hybrid Memory Technologies Using SOT-MRAM for on-Chip Cache Hierarchy. *IEEE Trans. Comput. Des. Integr. Circuits Syst.* **2015**, *34* (3), 367−380.

(8) Prenat, G.; Jabeur, K.; Vanhauwaert, P.; Pendina, G. Di; Oboril, F.; Bishnoi, R.; Ebrahimi, M.; Lamard, N.; Boulle, O.; Garello, K.; Langer, J.; Ocker, B.; Cyrille, M. C.; Gambardella, P.; Tahoori, M.; Gaudin, G. Ultra-Fast and High-Reliability SOT-MRAM: From Cache Replacement to Normally-Off Computing. *IEEE Trans. Multi-Scale Comput. Syst.* **2016**, *2* (1), 49−60.

(9) Peng, S.; Zhu, D.; Li, W.; Wu, H.; Grutter, A. J.; Gilbert, D. A.; Lu, J.; Xiong, D.; Cai, W.; Shafer, P.; Wang, K. L.; Zhao, W. Exchange Bias Switching in an Antiferromagnet/Ferromagnet Bilayer Driven by Spin-Orbit Torque. *Nat. Electron.* **2020**, *3* (12), 757−764.

(10) Liu, J.; Lu, J.; Peng, S.; Liu, Z.; Zhang, Y.; Qiao, J.; Wang, S.; Li, W.; Chen, J.; Wang, Z.; Li, R.-W.; Zhang, Y.; Zhao, W. Antiferromagnetic Materials: From Fundamentals to Applications. *Matter* **2025**, *8* (11), 102472.

(11) Liu, Z.; Peng, S.; Li, W.; Liu, J.; Lu, J.; Lu, S.; Xiong, D.; Cao, K.; Zhao, W. Robust Field-Free Voltage-Gated Spin-Orbit Torque Switching in IrMn-Based Perpendicular Magnetic Tunnel Junctions. *IEEE Electron Device Lett.* **2025**, *46* (5), 745−748.

(12) Das, S.; Chen, A.; Marinella, M. Beyond CMOS. *2021 IEEE International Roadmap for Devices and Systems Outbriefs*; IEEE, 2021; pp 1−129. DOI: 10.1109/IRDS54852.2021.00011.

(13) Grubišić-Čabo, A.; Guimarães, M. H. D.; Afanasiev, D.; Garcia Aguilar, J. H.; Aguilera, I.; Ali, M. N.; Bhattacharyya, S.; Blanter, Y. M.; Bosma, R.; Cheng, Z.; Dan, Z.; Dash, S. P.; Medina Dueñas, J.; Fernandez-Rossier, J.; Gibertini, M.; Grytsiuk, S.; Houmes, M. J. A.; Isaeva, A.; Knekna, C.; Kole, A. H.; Kurdi, S.; Lado, J. L.; Mañas-Valero, S.; Lopes, J. M. J.; Marian, D.; Na, M.; Pabst, F.; Barquero Pierantoni, S.; Regout, M.; Reho, R.; Rösner, M.; Sanz, D.; van der Sar, T.; Sławińska, J.; Verstraete, M. J.; Waseem, M.; van der Zant, H. S. J.; Zanolli, Z.; Soriano, D. Roadmap on Quantum Magnetic Materials. *2D Mater.* **2025**, *12* (3), 031501.

(14) Deng, Y.; Yu, Y.; Song, Y.; Zhang, J.; Wang, N. Z.; Sun, Z.; Yi, Y.; Wu, Y. Z.; Wu, S.; Zhu, J.; Wang, J.; Chen, X. H.; Zhang, Y. Gate-Tunable Room-Temperature Ferromagnetism in Two-Dimensional Fe3GeTe2. *Nature* **2018**, *563* (7729), 94−99.

(15) May, A. F.; Ovchinnikov, D.; Zheng, Q.; Hermann, R.; Calder, S.; Huang, B.; Fei, Z.; Liu, Y.; Xu, X.; McGuire, M. A. Ferromagnetism Near Room Temperature in the Cleavable van Der Waals Crystal Fe5GeTe2. *ACS Nano* **2019**, *13* (4), 4436−4442.

(16) Seo, J.; Kim, D. Y.; An, E. S.; Kim, K.; Kim, G.-Y.; Hwang, S.-Y.; Kim, D. W.; Jang, B. G.; Kim, H.; Eom, G.; Seo, S. Y.; Stania, R.; Muntwiler, M.; Lee, J.; Watanabe, K.; Taniguchi, T.; Jo, Y. J.; Lee, J.; Min, B., Il; Jo, M. H.; Yeom, H. W.; Choi, S.-Y.; Shim, J. H.; Kim, J. S. Nearly Room Temperature Ferromagnetism in a Magnetic Metal-Rich van Der Waals Metal. *Sci. Adv.* **2020**, *6* (3), No. eaay8912.

(17) May, A. F.; Du, M.-H.; Cooper, V. R.; McGuire, M. A. Tuning Magnetic Order in the van Der Waals Metal Fe5GeTe2 by Cobalt Substitution. *Phys. Rev. Mater.* **2020**, *4* (7), 074008.

(18) Zhang, G.; Guo, F.; Wu, H.; Wen, X.; Yang, L.; Jin, W.; Zhang, W.; Chang, H. Above-Room-Temperature Strong Intrinsic Ferromagnetism in 2D van Der Waals Fe3GaTe2 with Large Perpendicular Magnetic Anisotropy. *Nat. Commun.* **2022**, *13* (1), 5067.

(19) Tian, C.; Pan, F.; Xu, S.; Ai, K.; Xia, T.; Cheng, P. Tunable Magnetic Properties in van Der Waals Crystals (Fe1-xCox)5GeTe2. *Appl. Phys. Lett.* **2020**, *116* (20), 202402.

(20) Ohta, T.; Kurokawa, K.; Jiang, N.; Yamagami, K.; Okada, Y.; Niimi, Y. Enhancement of Spin-Flop-Induced Magnetic Hysteresis in van Der Waals Magnet $(Fe_{1-x}Co_x)_5GeTe_2$. *Appl. Phys. Lett.* **2023**, *122* (15). DOI: 10.1063/5.0141495.

(21) Chen, X.; Schierle, E.; He, Y.; Vranas, M.; Freeland, J. W.; McChesney, J. L.; Ramesh, R.; Birgeneau, R. J.; Frano, A. Antiferromagnetic Order in Co-Doped Fe5GeTe2 Probed by Resonant Magnetic x-Ray Scattering. *Phys. Rev. Mater.* **2022**, *6* (9), 094404.

(22) Ngaloy, R.; Zhao, B.; Ershadrad, S.; Gupta, R.; Davoudiniya, M.; Bainsla, L.; Sjöström, L.; Hoque, M. A.; Kalaboukhov, A.; Svedlindh, P.; Sanyal, B.; Dash, S. P. Strong In-Plane Magnetization and Spin Polarization in (Co0.15Fe0.85)5GeTe2/Graphene van Der Waals Heterostructure Spin-Valve at Room Temperature. *ACS Nano* **2024**, *18* (7), 5248.

(23) Zhao, B.; Ngaloy, R.; Ghosh, S.; Ershadrad, S.; Gupta, R.; Ali, K.; Hoque, A. M.; Karpiak, B.; Khokhriakov, D.; Polley, C.; Thiagarajan, B.; Kalaboukhov, A.; Svedlindh, P.; Sanyal, B.; Dash, S. P. A Room-Temperature Spin-Valve with van Der Waals Ferromagnet Fe5GeTe2/Graphene Heterostructure. *Adv. Mater.* **2023**, *35* (16), 2209113.

(24) Zhang, H.; Raftrey, D.; Chan, Y.-T.; Shao, Y.-T.; Chen, R.; Chen, X.; Huang, X.; Reichanadter, J. T.; Dong, K.; Susarla, S.; Caretta, L.; Chen, Z.; Yao, J.; Fischer, P.; Neaton, J. B.; Wu, W.; Muller, D. A.; Birgeneau, R. J.; Ramesh, R. Room-Temperature Skyrmion Lattice in a Layered Magnet (Fe0.5Co0.5)5GeTe2. *Sci. Adv.* **2022**, *8* (12), No. eabm7103.

(25) Zhao, B.; Ngaloy, R.; Sjostrom, L.; Dash, S. P. A Spin-Texture Spin-Valves With Van Der Waals Magnets. *Advanced Science* **2026**, *13*, e00041.

(26) Zhao, B.; Bainsla, L.; Ershadrad, S.; Zeng, L.; Ngaloy, R.; Svedlindh, P.; Olsson, E.; Sanyal, B.; Dash, S. P. Coexisting Non-Trivial Van Der Waals Magnetic Orders Enable Field-Free Spin-Orbit Torque Magnetization Dynamics. *Adv. Mater.* **2025**, *37* (37), 2502822.

(27) Wang, Z.; Sapkota, D.; Taniguchi, T.; Watanabe, K.; Mandrus, D.; Morpurgo, A. F. Tunneling Spin Valves Based on Fe3GeTe2/HBN/Fe3GeTe2 van Der Waals Heterostructures. *Nano Lett.* **2018**, *18* (7), 4303−4308.

(28) Chen, Y.; Samanta, K.; Shahed, N. A.; Zhang, H.; Fang, C.; Ernst, A.; Tsymbal, E. Y.; Parkin, S. S. P. Twist-Assisted All-Antiferromagnetic Tunnel Junction in the Atomic Limit. *Nature* **2024**, *632* (8027), 1045−1051.

(29) Albarakati, S.; Tan, C.; Chen, Z.; Partridge, J. G.; Zheng, G.; Farrar, L.; Mayes, E. L. H.; Field, M. R.; Lee, C.; Wang, Y.; Xiong, Y.; Tian, M.; Xiang, F.; Hamilton, A. R.; Tretiakov, O. A.; Culcer, D.; Zhao, Y.; Wang, L. Antisymmetric Magnetoresistance in van Der Waals Fe3GeTe2/Graphite/Fe3GeTe2 Trilayer Heterostructures. *Sci. Adv.* **2019**, *5* (7), No. eaaw0409.

(30) Kao, I.-H.; Muzzio, R.; Zhang, H.; Zhu, M.; Gobbo, J.; Yuan, S.; Weber, D.; Rao, R.; Li, J.; Edgar, J. H.; Goldberger, J. E.; Yan, J.; Mandrus, D. G.; Hwang, J.; Cheng, R.; Katoch, J.; Singh, S. Deterministic Switching of a Perpendicularly Polarized Magnet Using Unconventional Spin-Orbit Torques in WTe2. *Nat. Mater.* **2022**, *21* (9), 1029−1034.
(31) Alghamdi, M.; Lohmann, M.; Li, J.; Jothi, P. R.; Shao, Q.; Aldosary, M.; Su, T.; Fokwa, B. P. T.; Shi, J. Highly Efficient Spin-Orbit Torque and Switching of Layered Ferromagnet Fe3GeTe2. *Nano Lett.* **2019**, *19* (7), 4400−4405.
(32) Wang, X.; Tang, J.; Xia, X.; He, C.; Zhang, J.; Liu, Y.; Wan, C.; Fang, C.; Guo, C.; Yang, W.; Guang, Y.; Zhang, X.; Xu, H.; Wei, J.; Liao, M.; Lu, X.; Feng, J.; Li, X.; Peng, Y.; Wei, H.; Yang, R.; Shi, D.; Zhang, X.; Han, Z.; Zhang, Z.; Zhang, G.; Yu, G.; Han, X. Current-Driven Magnetization Switching in a van Der Waals Ferromagnet Fe3GeTe2. *Sci. Adv.* **2019**, *5* (8), No. eaaw8904.
(33) Li, W.; Zhu, W.; Zhang, G.; Wu, H.; Zhu, S.; Li, R.; Zhang, E.; Zhang, X.; Deng, Y.; Zhang, J.; Zhao, L.; Chang, H.; Wang, K. Room-Temperature van Der Waals Ferromagnet Switching by Spin-Orbit Torques. *Adv. Mater.* **2023**, *35* (51), 2303688.
(34) Kajale, S. N.; Nguyen, T.; Chao, C. A.; Bono, D. C.; Boonkird, A.; Li, M.; Sarkar, D. Current-Induced Switching of a van Der Waals Ferromagnet at Room Temperature. *Nat. Commun.* **2024**, *15* (1), 1485.
(35) Pandey, L.; Zhao, B.; Tenzin, K.; Ngaloy, R.; Lamparská, V.; Bangar, H.; Ali, A.; Abdel-Hafiez, M.; Zhang, G.; Wu, H.; Chang, H.; Sjöström, L.; Rout, P.; Sławińska, J.; Dash, S. P. Tunable Unconventional Spin Orbit Torque Magnetization Dynamics in van Der Waals Heterostructures. *Nat. Commun.* **2025**, *16* (1), 8722.
(36) Liu, L.; Moriyama, T.; Ralph, D. C.; Buhrman, R. A. Spin-Torque Ferromagnetic Resonance Induced by the Spin Hall Effect. *Phys. Rev. Lett.* **2011**, *106* (3), 036601.
(37) Demasius, K.-U.; Phung, T.; Zhang, W.; Hughes, B. P.; Yang, S.-H.; Kellock, A.; Han, W.; Pushp, A.; Parkin, S. S. P. Enhanced Spin-Orbit Torques by Oxygen Incorporation in Tungsten Films. *Nat. Commun.* **2016**, *7* (1), 10644.
(38) Bainsla, L.; Zhao, B.; Behera, N.; Hoque, A. M.; Sjöström, L.; Martinelli, A.; Abdel-Hafiez, M.; Åkerman, J.; Dash, S. P. Large Out-of-Plane Spin-Orbit Torque in Topological Weyl Semimetal TaIrTe4. *Nat. Commun.* **2024**, *15* (1), 4649.
(39) MacNeill, D.; Stiehl, G. M.; Guimaraes, M. H. D.; Buhrman, R. A.; Park, J.; Ralph, D. C. Control of Spin-Orbit Torques through Crystal Symmetry in WTe2/Ferromagnet Bilayers. *Nat. Phys.* **2017**, *13* (3), 300−305.
(40) Kittel, C. On the Theory of Ferromagnetic Resonance Absorption. *Phys. Rev.* **1948**, *73* (2), 155−161.
(41) Bainsla, L.; Kumar, A.; Awad, A. A.; Wang, C.; Zahedinejad, M.; Behera, N.; Fulara, H.; Khymyn, R.; Houshang, A.; Weissenrieder, J.; Åkerman, J. Ultrathin Ferrimagnetic GdFeCo Films with Low Damping. *Adv. Funct. Mater.* **2022**, *32* (23), 2111693.
(42) Li, D.; Chen, S.; Zuo, Y.; Yun, J.; Cui, B.; Wu, K.; Guo, X.; Yang, D.; Wang, J.; Xi, L. Roles of Joule Heating and Spin-Orbit Torques in the Direct Current Induced Magnetization Reversal. *Sci. Reports 2018 81* **2018**, *8* (1), 1−11.
(43) Bose, A.; Schreiber, N. J.; Jain, R.; Shao, D.-F.; Nair, H. P.; Sun, J.; Zhang, X. S.; Muller, D. A.; Tsymbal, E. Y.; Schlom, D. G.; Ralph, D. C. Tilted Spin Current Generated by the Collinear Antiferromagnet Ruthenium Dioxide. *Nat. Electron.* **2022**, *5* (5), 267−274.
(44) Baek, S. H. C.; Amin, V. P.; Oh, Y. W.; Go, G.; Lee, S. J.; Lee, G. H.; Kim, K. J.; Stiles, M. D.; Park, B. G.; Lee, K. J. Spin Currents and Spin-Orbit Torques in Ferromagnetic Trilayers. *Nat. Mater. 2018 176* **2018**, *17* (6), 509−513.
(45) Liu, Y.; Shi, G.; Kumar, D.; Kim, T.; Shi, S.; Yang, D.; Zhang, J.; Zhang, C.; Wang, F.; Yang, S.; Pu, Y.; Yu, P.; Cai, K.; Yang, H. Field-Free Switching of Perpendicular Magnetization at Room Temperature Using out-of-Plane Spins from TaIrTe4. *Nat. Electron.* **2023**, *6* (10), 732−738.
(46) Wang, F.; Shi, G.; Kim, K.-W.; Park, H.-J.; Jang, J. G.; Tan, H. R.; Lin, M.; Liu, Y.; Kim, T.; Yang, D.; Zhao, S.; Lee, K.; Yang, S.; Soumyanarayanan, A.; Lee, K.-J.; Yang, H. Field-Free Switching of Perpendicular Magnetization by Two-Dimensional PtTe2/WTe2 van Der Waals Heterostructures with High Spin Hall Conductivity. *Nat. Mater.* **2024**, *23* (6), 768−774.
(47) Pai, C.-F.; Ou, Y.; Vilela-Leão, L. H.; Ralph, D. C.; Buhrman, R. A. Dependence of the Efficiency of Spin Hall Torque on the Transparency of Pt/Ferromagnetic Layer Interfaces. *Phys. Rev. B* **2015**, *92* (6), 064426.
(48) Nguyen, M.-H.; Ralph, D. C.; Buhrman, R. A. Spin Torque Study of the Spin Hall Conductivity and Spin Diffusion Length in Platinum Thin Films with Varying Resistivity. *Phys. Rev. Lett.* **2016**, *116* (12), 126601.
(49) Zhao, B.; Pandey, L.; Ali, K.; Wang, E.; Polley, C. M.; Thiagarajan, B.; Makk, P.; Guimarães, M. H. D.; Dash, S. P. Field-Free Spin-Orbit Torque Switching of Canted van Der Waals Magnets. *ACS Nano* **2025**, *19* (14), 13817−13824.
(50) Humphries, A. M.; Wang, T.; Edwards, E. R. J.; Allen, S. R.; Shaw, J. M.; Nembach, H. T.; Xiao, J. Q.; Silva, T. J.; Fan, X. Observation of Spin-Orbit Effects with Spin Rotation Symmetry. *Nat. Commun. 2017 81* **2017**, *8* (1), 1−7.
(51) Amin, V. P.; Zemen, J.; Stiles, M. D. Interface-Generated Spin Currents. *Phys. Rev. Lett.* **2018**, *121* (13), 136805.
(52) Choi, G.; Ryu, J.; Lee, S.; Kang, J.; Noh, N.; Yuk, J. M.; Park, B. Thickness Dependence of Interface-Generated Spin Currents in Ferromagnet/Ti/CoFeB Trilayers. *Adv. Mater. Interfaces* **2022**, *9* (36), 2201317.
(53) Zhao, B.; Karpiak, B.; Khokhriakov, D.; Johansson, A.; Hoque, A. M.; Xu, X.; Jiang, Y.; Mertig, I.; Dash, S. P. Unconventional Charge-Spin Conversion in Weyl-Semimetal WTe2. *Adv. Mater.* **2020**, *32* (38), 2000818.
(54) Shi, S.; Li, J.; Hsu, C.; Lee, K.; Wang, Y.; Yang, L.; Wang, J.; Wang, Q.; Wu, H.; Zhang, W.; Eda, G.; Liang, G.; Chang, H.; Yang, H. Observation of the Out-of-Plane Polarized Spin Current from CVD Grown WTe2. *Adv. Quantum Technol.* **2021**, *4* (8), 2100038.
(55) Zhang, Y.; Xu, H.; Jia, K.; Lan, G.; Huang, Z.; He, B.; He, C.; Shao, Q.; Wang, Y.; Zhao, M.; Ma, T.; Dong, J.; Guo, C.; Cheng, C.; Feng, J.; Wan, C.; Wei, H.; Shi, Y.; Zhang, G.; Han, X.; Yu, G. Room Temperature Field-Free Switching of Perpendicular Magnetization through Spin-Orbit Torque Originating from Low-Symmetry Type II Weyl Semimetal. *Sci. Adv.* **2023**, *9* (44), adg9819.
(56) Zhang, Y.; Ren, X.; Liu, R.; Chen, Z.; Wu, X.; Pang, J.; Wang, W.; Lan, G.; Watanabe, K.; Taniguchi, T.; Shi, Y.; Yu, G.; Shao, Q. Robust Field-Free Switching Using Large Unconventional Spin-Orbit Torque in an All-Van Der Waals Heterostructure. *Adv. Mater.* **2024**, *36* (41), 2406464.
(57) Stiehl, G. M.; Li, R.; Gupta, V.; Baggari, I. El; Jiang, S.; Xie, H.; Kourkoutis, L. F.; Mak, K. F.; Shan, J.; Buhrman, R. A.; Ralph, D. C. Layer-Dependent Spin-Orbit Torques Generated by the Centrosymmetric Transition Metal Dichalcogenide B-MoTe2. *Phys. Rev. B* **2019**, *100* (18), 184402.
(58) Kimata, M.; Chen, H.; Kondou, K.; Sugimoto, S.; Muduli, P. K.; Ikhlas, M.; Omori, Y.; Tomita, T.; MacDonald, A. H.; Nakatsuji, S.; Otani, Y. Magnetic and Magnetic Inverse Spin Hall Effects in a Non-Collinear Antiferromagnet. *Nat. 2019 5657741* **2019**, *565* (7741), 627−630.
(59) Chen, X.; Shi, S.; Shi, G.; Fan, X.; Song, C.; Zhou, X.; Bai, H.; Liao, L.; Zhou, Y.; Zhang, H.; Li, A.; Chen, Y.; Han, X.; Jiang, S.; Zhu, Z.; Wu, H.; Wang, X.; Xue, D.; Yang, H.; Pan, F. Observation of the Antiferromagnetic Spin Hall Effect. *Nat. Mater. 2021 206* **2021**, *20* (6), 800−804.
(60) Hu, S.; Shao, D.-F.; Yang, H.; Pan, C.; Fu, Z.; Tang, M.; Yang, Y.; Fan, W.; Zhou, S.; Tsymbal, E. Y.; Qiu, X. Efficient Perpendicular Magnetization Switching by a Magnetic Spin Hall Effect in a Noncollinear Antiferromagnet. *Nat. Commun.* **2022**, *13* (1), 4447.
(61) Alahmed, L.; Nepal, B.; Macy, J.; Zheng, W.; Casas, B.; Sapkota, A.; Jones, N.; Mazza, A. R.; Brahlek, M.; Jin, W.; Mahjouri-Samani, M.; Zhang, S. S. L.; Mewes, C.; Balicas, L.; Mewes, T.; Li, P. Magnetism and Spin Dynamics in Room-Temperature van Der Waals Magnet Fe5GeTe2. *2D Mater.* **2021**, *8* (4), 045030.

(62) Ni, L.; Chen, Z.; Li, W.; Lu, X.; Yan, Y.; Zhang, L.; Yan, C.; Chen, Y.; Gu, Y.; Li, Y.; Zhang, R.; Zhai, Y.; Liu, R.; Yang, Y.; Xu, Y. Magnetic Dynamics of Two-Dimensional Itinerant Ferromagnet Fe3GeTe2 *. *Chinese Phys. B* **2021**, *30* (9), 097501.
(63) Sandler, G. M.; Bertram, H. N.; Silva, T. J.; Crawford, T. M. Determination of the Magnetic Damping Constant in NiFe Films. *J. Appl. Phys.* **1999**, *85* (8), 5080−5082.
(64) Zhao, Y.; Song, Q.; Yang, S.-H.; Su, T.; Yuan, W.; Parkin, S. S. P.; Shi, J.; Han, W. Experimental Investigation of Temperature-Dependent Gilbert Damping in Permalloy Thin Films. *Sci. Rep.* **2016**, *6* (1), 22890.
(65) Iihama, S.; Mizukami, S.; Naganuma, H.; Oogane, M.; Ando, Y.; Miyazaki, T. Gilbert Damping Constants of Ta/CoFeB/MgO(Ta) Thin Films Measured by Optical Detection of Precessional Magnetization Dynamics. *Phys. Rev. B - Condens. Matter Mater. Phys.* **2014**, *89* (17), 174416.
(66) Okada, A.; Kanai, S.; Yamanouchi, M.; Ikeda, S.; Matsukura, F.; Ohno, H. Electric-Field Effects on Magnetic Anisotropy and Damping Constant in Ta/CoFeB/MgO Investigated by Ferromagnetic Resonance. *Appl. Phys. Lett.* **2014**, *105* (5). DOI: 10.1063/1.4892824.
(67) Zhao, B.; Ngaloy, R.; Pandey, L.; Bangar, H.; Dubey, D. P.; Dash, S. P. Nanoelectronics with Two Dimensional Magnets. *Nano Lett.* **2026**, *26*, 7209.

https://doi.org/10.1021/acs.nanolett.6c02494
Nano Lett. XXXX, XXX, XXX−XXX